On the Synthesis of the Astronomically Elusive 1-Ethynyl-3-Silacyclopropenylidene (c-SiC$_4$H$_2$) Molecule in Circumstellar Envelopes of Carbon-rich Asymptotic Giant Branch Stars and Its Potential Role in the Formation of the Silicon Tetracarbide Chain (SiC$_4$)

Zhenghai Yang[1,4], Srinivas Doddipatla[1], Ralf I. Kaiser[1] , Anatoliy A. Nikolayev[2,4], Valeriy N. Azyazov[2], and Alexander M. Mebel[3]

[1] Department of Chemistry, University of Hawai'i at Manoa, Honolulu, HI 96822, USA; ralfk@hawaii.edu
[2] Lebedev Physical Institute, Samara 443011 and Samara National Research University, Samara 443086, Russia
[3] Department of Chemistry and Biochemistry, Florida International University, Miami, FL 33199, USA; mebela@fiu.edu

Abstract

Organosilicon molecules such as silicon carbide (SiC), silicon dicarbide (c-SiC$_2$), silicon tricarbide (c-SiC$_3$), and silicon tetracarbide (SiC$_4$) represent basic molecular building blocks connected to the growth of silicon-carbide dust grains in the outflow of circumstellar envelopes of carbon-rich asymptotic giant branch (AGB) stars. Yet, the fundamental mechanisms of the formation of silicon carbides and of the early processes that initiate the coupling of silicon–carbon bonds in circumstellar envelopes have remained obscure. Here, we reveal in a crossed molecular beam experiment contemplated with ab initio electronic calculations that the astronomically elusive 1-ethynyl-3-silacyclopropenylidene molecule (c-SiC$_4$H$_2$, C$_s$, X^{1}A′) can be synthesized via a single-collision event through the barrierless reaction of the silylidyne radical (SiH) with diacetylene (C$_4$H$_2$). This system represents a benchmark of a previously overlooked class of reactions, in which the silicon–carbon bond coupling can be initiated by a barrierless and overall exergic reaction between the simplest silicon-bearing radical (silylidyne) and a highly hydrogen-deficient hydrocarbon (diacetylene) in the inner circumstellar envelopes of evolved carbon-rich stars such as IRC+10216. Considering that organosilicon molecules like 1-ethynyl-3-silacyclopropenylidene might be ultimately photolyzed to bare carbon–silicon clusters like the linear silicon tetracarbide (SiC$_4$), hydrogenated silicon–carbon clusters might represent the missing link eventually connecting simple molecular precursors such as silane (SiH$_4$) to the population of silicon-carbide based interstellar grains ejected from carbon-rich AGB stars into the interstellar medium.

Unified Astronomy Thesaurus concepts: Astrochemistry (75); Interstellar dust (836); Laboratory astrophysics (2004); Circumstellar envelopes (237)

1. Introduction

Since the discovery of the C$_{2v}$ symmetric, cyclic silicon dicarbide molecule (c-SiC$_2$) by Merrill and Sanford nearly 100 years ago toward carbon-rich asymptotic giant branch (AGB) stars via emission features between 410 and 550 nm (Merrill 1926; Sanford 1926), silicon carbides like silicon monocarbide (Bernath et al. 1988) silicon dicarbide (c-SiC$_2$; Massalkhi et al. 2018), disilicon monocarbide (Si$_2$C; Weltner & McLeod 1964), silicon tricarbide (c-SiC$_3$; Apponi et al. 1999), and silicon tetracarbide (SiC$_4$; Ohishi et al. 1989; Figure 1) have received considerable interest from the astronomy, laboratory astrophysics, and physical chemistry communities (Ziurys 2006). This is due to the role of (hydrogenated precursors of) silicon-carbide molecules in the chemical evolution of the interstellar medium (ISM) and their link to the formation of silicon-carbide dust grains in the outflow of circumstellar envelopes of carbon-rich AGB stars like IRC+10216 (McCarthy et al. 2003; Velilla-Prieto et al. 2018). Dust formation in AGB stars is a poorly understood process (McCarthy et al. 2019) with carbon-rich outflows suggested as a critical source of silicon-carbide-based interstellar grains with sizes of up to a few 100 nm. The formation of these grains is proposed to be efficiently initiated at temperatures of 1000–2500 K within the first few stellar radii

with overall gas densities of 10^8–10^{14} cm^{-3} (McCarthy et al. 2019). This is well documented through the observation of ubiquitous infrared emission feature in the spectra of multiple carbon stars close to 11.0 μm (909 cm^{-1}), which has been assigned to silicon-carbide dust grains (Speck et al. 1997; Ziurys 2006). Due to the simultaneous abundance of silicon-carbide molecules (SiC$_n$; $n = 1$–4; Thaddeus et al. 1984; McCarthy et al. 2003), organosilicon clusters have been contemplated as fundamental molecular building blocks in the synthesis of more complex silicon-bearing molecules and ultimately of silicon-carbide grains (Ohishi et al. 1989). Refined ^{13}C/^{12}C isotope analysis confirmed that the silicon-carbide stardust recovered from meteorites such as presolar grains is sourced in carbon-rich AGB stars (Zinner 1995) with smaller fractions originating from SNe II and novae (Zinner 1998; Zinner et al. 2006).

However, the underlying molecular processes, which initiate and connect the circumstellar silicon and carbon chemistries to the formation of sub micrometer-sized grains, are not well understood (Cherchneff et al. 2000; Decin et al. 2008; Cherchneff 2012). Early models proposed complex reaction networks dictated by ion–molecule reactions, radiative associations, and dissociative recombination with either atomic or singly ionized silicon (Millar & Herbst 1994; Lis et al. 2006; Wakelam et al. 2010). However, these models could not replicate the astronomical observations of even the simplest

---
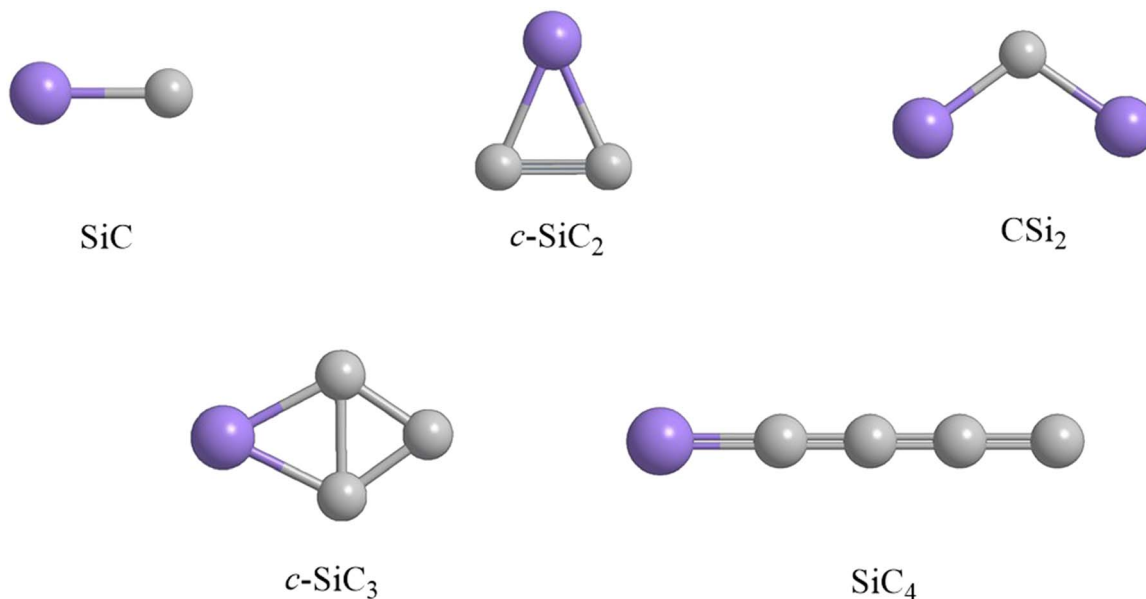[4] Contributed equally to this work.

Figure 1. Silicon–carbon clusters as detected in the circumstellar envelope of IRC+10216.

silicon carbides (SiC, c-SiC$_2$) in the circumstellar shell of IRC +10216 predicting column densities of up to two orders of magnitude lower compared to the observations (McElroy et al. 2013; Li et al. 2014). Recent models propose stepwise molecular growth processes commencing with silicon monocarbide (Ríos et al.) and silicon dicarbide (c-SiC$_2$; Yasuda & Kozasa 2012). Further chemical growth of silicon-carbide dust is suggested to involve reactions with the ethynyl radical (C$_2$H), acetylene (C$_2$H$_2$), and diacetylene (C$_4$H$_2$Yasuda & Kozasa 2012). However, the source of silicon incorporated into the silicon-carbide molecules is still unknown. Silane (SiH$_4$)—the simplest closed shell hydride of silicon—has been observed toward IRC+10216 (Goldhaber & Betz 1984). Upon photolysis close to the photosphere, silane can be efficiently photodissociated (Suto & Lee 1986) to the silylidyne radical (SiH), which may subsequently react rapidly with unsaturated hydrocarbons such as acetylene and diacetylene in the envelope (Parker et al. 2013). Nevertheless, the elucidation of the validity of these reaction mechanisms has only scratched the surface leading solely to the formation of hydrogenated organosilicon molecules carrying one silicon atom along with only two (SiC$_2$H$_2$) (Parker et al. 2013) or three (SiC$_3$H$_4$, SiC$_3$H$_2$) (Yang et al. 2015, 2019) carbon atoms. Although these hydrogenated species may represent reactive intermediates to silicon dicarbide (c-SiC$_2$) and silicon tricarbide (c-SiC$_3$) upon photolysis accompanied by dehydrogenation, these reactions cannot account for any (hydrogenated) organosilicon precursors leading to truly complex silicon carbides such as linear silicon tetracarbide molecule (SiC$_4$) upon photofragmentation. McCarthy et al. observed the rotational spectrum of 1-sila-1,2,3,4-pentatetraenylidene (H$_2$SiC$_4$; H$_2$CCCCSi)—a potential precursor to silicon tetracarbide (SiC$_4$; SiCCCC) in a discharge process of silane and diacetylene gas mixtures in a pulsed supersonic molecular beam by Fourier transform microwave spectroscopy (Figure 2; McCarthy & Thaddeus 2002). In elegant matrix isolation studies, Maier and coworkers trapped diethynylsilylidene (HCCSiCCH) and 1-ethynyl-3-silacyclopropenylidene molecule (c-SiC$_2$HCCH) at 10 K (Maier et al. 1998). Very recently, Job et al. revealed

computationally the existence of 11 SiC$_4$H$_2$ isomers, among them 1-sila-1,2,3,4-pentatetraenylidene (H$_2$CCCCSi), diethynylsilylidene (HCCSiCCH), 1,3-butadiynylsilylidene (HCCCCSiH), and 1-ethynyl-3-silacyclopropenylidene (c-SiC$_2$HCCH) already identified in the laboratory (Job et al. 2020). Nevertheless, the fundamental reaction pathways leading to *any* H$_2$SiC$_4$ isomer under conditions replicating the chemical makeup and temperature in circumstellar envelopes of carbon stars have remained elusive.

Here, we reveal the results of a crossed molecular beam experiment of the silylidyne radical (SiH; X$^2\Pi$) with diacetylene (C$_4$H$_2$, X$^1\Sigma_g^+$). Combining the reactive scattering data with electronic structure calculations, we provide compelling evidence on the formation of the astronomically elusive 1-ethynyl-3-silacyclopropenylidene molecule (p1, C$_s$, X^{1}A′) via a single-collision event through the barrierless reaction of two neutral molecules: the silylidyne radical and diacetylene. The silylidyne–diacetylene system represents a benchmark of a previously unnoticed reaction class leading to the synthesis of hydrogen-deficient organosilicon molecules commenced through barrierless reactions of silylidyne radicals with alkynes—unsaturated hydrocarbons carrying the −C≡C–H moiety—in circumstellar envelopes of evolved carbon stars such as IRC+10216. The experiments were carried out at a collision energy of 31 kJ mol^{-1} corresponding to a temperature of about 3500 K. This is representative of temperatures in the circumstellar envelopes of carbon-rich stars such as IRC +10216 within the first few stellar radii to the photosphere reaching temperatures up to a few 1000 K thus mimicking the physical (temperature) and chemical (reactant) conditions in circumstellar envelopes of carbon-rich AGB stars. Within two stellar radii, both the silylidyne radical (SiH) and diacetylene (C$_4$H$_2$) reactants are predicted to be present at fractional abundances of up to 2×10^{-7} and 2.4×10^{-8}, respectively (Willacy & Cherchneff 1998). The facile route to 1-ethynyl-3-silacyclopropenylidene (c-SiC$_4$H$_2$), as an ethynyl (−C≡C–H) substituted silacyclopropenylidene (c-SiC$_2$H$_2$) species, offers a versatile route to synthesize hydrogen-deficient organosilicon molecules. These might be photolyzed eventually to the bare carbon–silicon clusters such as c-SiC$_2$ (Maier et al. 1994;
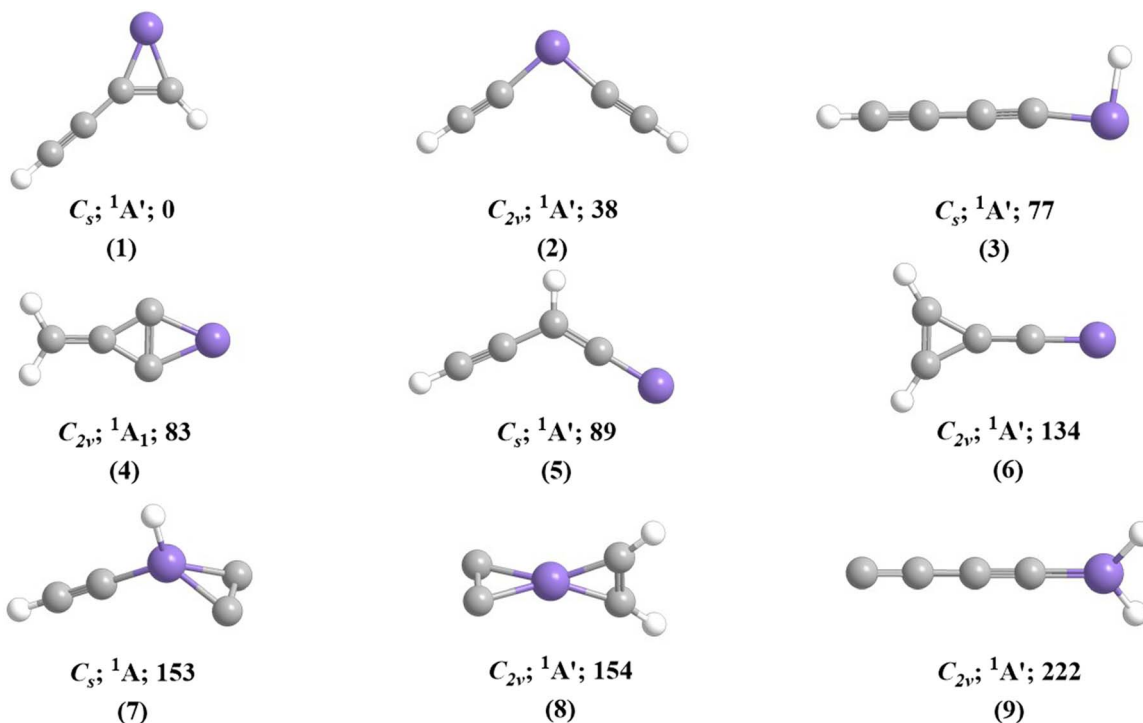
Figure 2. Low-energy SiC_4H_2 isomers along with their point groups and ground-state electronic wave functions. Relative energies calculated at the CCSD(T)-F12/cc-pVQZ-f12//ωB97XD/6-311G(d,p) + ZPE(ωB97XD/6-311G(d,p)) level are given in kJ mol^{-1}.

Redman et al. 2003), c-SiC_3 (Yang et al. 2019), and l-C_4Si (McCarthy & Thaddeus 2002) through the loss of hydrogen hence leading to molecules contemplated as critical building blocks of silicon-carbide based interstellar grains.

2. Results

2.1. Crossed Molecular Beams Studies—Laboratory and Center-of-mass (CM) Frame

The reaction of the silylidyne radical (SiH; $X^2\Pi$) with diacetylene (C_4H_2, $X^1\Sigma_g^+$) was conducted under single-collision conditions in the gas phase utilizing the crossed molecular beam approach. Considering the natural isotope abundances of silicon [^{28}Si (92.2%), ^{29}Si (4.7%), ^{30}Si (3.1%)] and of carbon [^{12}C (98.9%), ^{13}C (1.1%)], reactive scattering signal was probed from mass-to-charge (m/z) of $m/z = 80$ (^{30}SiC$_4$H$_2^+$) to $m/z = 76$ (^{28}SiC$_4^+$), signal at $m/z = 77$ (^{28}SiC$_4$H$^+$, ^{29}SiC$_4^+$, ^{28}Si^{13}CC$_3^+$) was collected at level of $63\% \pm 3\%$ compared to signal at $m/z = 78$ (^{28}SiC$_4$H$_2^+$, ^{29}SiC$_4$H$^+$, ^{28}Si^{13}CC$_3$H$^+$, ^{30}SiC$_4^+$). No signal was detected at $m/z = 76$, 79 and 80. It is important to note that the time-of-flight (TOF) spectra recorded at $m/z = 77$ and 78 reveal identical patterns after scaling, indicating the existence of a single channel, namely the formation of ^{28}SiC$_4$H$_2$ (78 amu; hereafter; SiC_4H_2) along with hydrogen atom (H; 1 amu), and the signal at $m/z = 77$ originate from dissociative ionization of the SiC_4H_2 in the electron impact ionizer. Therefore, the laboratory data alone offer compelling evidence on the formation of SiC_4H_2 plus atomic hydrogen in the reaction of ground-state silylidyne radicals with diacetylene. The laboratory angular distribution obtained at $m/z = 78$ is nearly forward–backward symmetric around the CM angle of $31°.5 \pm 0°.1$ and spread over $20°$ (Figure 3). These results propose indirect scattering dynamics through the formation of SiC_4H_3 intermediate(s).

The prime goal of our study is to unravel the nature of the SiC_4H_2 isomer(s) formed and the underlying reaction mechanism(s). This requires a transformation of the laboratory data (TOF spectra, laboratory angular distribution) into the CM reference frame resulting in the CM translational energy $P(E_T)$ and angular flux $T(\theta)$ (Figure 4). The laboratory data could be replicated with a single channel fit with the mass combination of 78 amu (SiC_4H_2) and 1 amu (H). For those reaction products formed without internal excitation, the high-energy cutoff of the $P(E_T)$ of 45 ± 5 kJ mol^{-1} signifies the sum of the reaction exoergicity plus the collision energy (31.2 ± 0.2 kJ mol^{-1}). A subtraction of the collision energy reveals that the reaction is exoergic by 14 ± 5 kJ mol^{-1}. This value is in excellent agreement with our computed value for an exoergic reaction of 17 ± 3 kJ mol^{-1} to synthesize the 1-ethynyl-3-silacyclopropenylidene isomer (1) along with atomic hydrogen (Figures 4 and 5). As for the thermodynamically less-stable isomers (2)–(7), isomers (3)–(7) are energetically not accessible considering the collision energy; (2) might be "hidden" in the low-energy tail of the $P(E_T)$ and hence might represent a minor product. Consequently, we deduce that the 1-ethynyl-3-silacyclopropenylidene molecule (1) is formed in the reaction of the silylidyne radical with diacetylene. Additionally, the translational energy distribution is peaking close to zero translational energy, revealing that the emission of the hydrogen atom is likely associated with a rather loose exit transition state via a simple bond-rupture process. Further, the energy channeled on average into the translational degrees of freedom of the final products is only $25\% \pm 5\%$ proposing indirect scattering dynamics via the unimolecular decomposition of a SiC_4H_3 complex(es). Finally, the CM angular distribution $T(\theta)$ shows intensity over the complete angular range and a forward–backward symmetric distribution; this also suggests an indirect, complex forming reaction mechanism (Levine 2009).
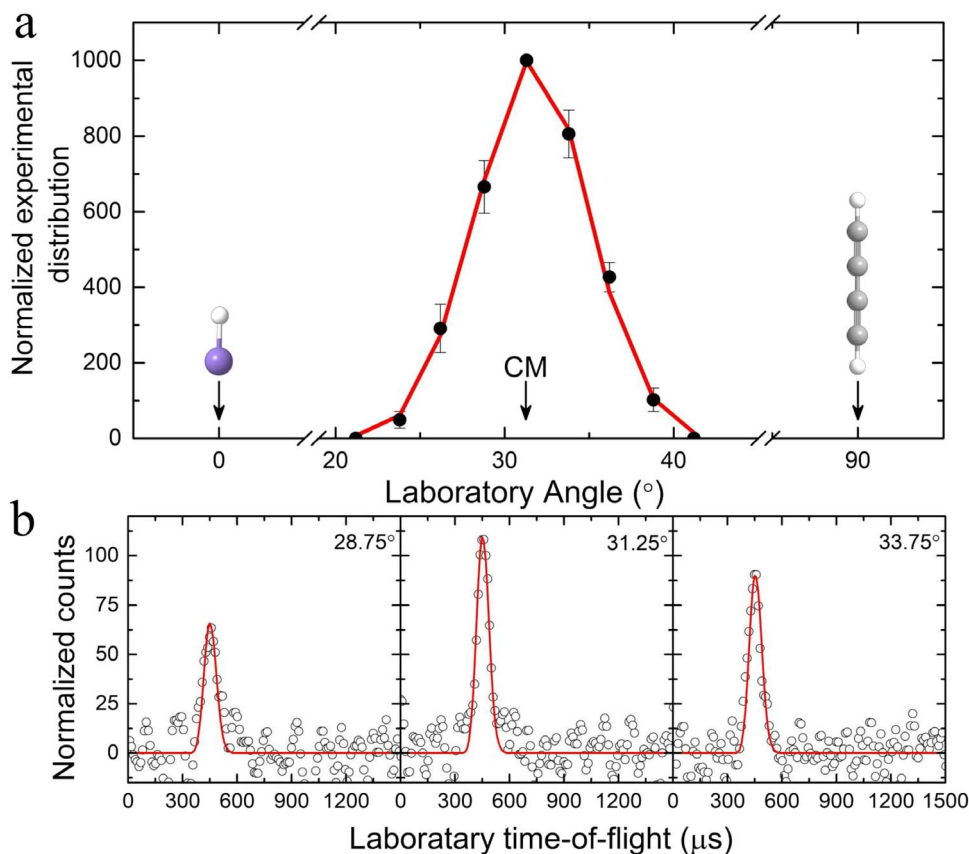
Figure 3. Laboratory angular distribution at mass-to-charge (m/z) of 78 ($SiC_4H_2^+$) recorded in the reaction of the silylidyne radical with diacetylene together with selected time-of-flight (TOF) spectra. Open circles indicate experimental data, and the solid red line indicates the calculated distribution with the best-fit center-of-mass (CM) functions as depicted in Figure 4. CM designates the center-of-mass angle.

2.2. Electronic Structure Calculations and Reaction Mechanism

The electronic structure calculations were performed at a level of theory sufficiently high enough to predict relative energies of the local minima and transition states within $8\,kJ\,mol^{-1}$, and reaction energies to a precision of $3\,kJ\,mol^{-1}$. The silylidyne radical can either add to double and/or triple bonds (π electron system) or may insert into single bonds (σ electron system). The addition to the terminal carbon atom of diacetylene leads to a doublet intermediate i1 (cis/trans), whereas an addition to both the carbon–carbon triple bond of C1 and C2 forms intermediate i2. Both addition pathways are barrierless leading to open shell doublet collision complexes stabilized by 88 and $91\,kJ\,mol^{-1}$ (cis-i1, C_s, $^2A'$), (trans-i1, C_1, ^2A) and $167\,kJ\,mol^{-1}$ (i2, C_1, ^2A), respectively. A barrier to ring closure of only $1\,kJ\,mol^{-1}$ separates the cis-i1 and trans-i1 with i2 collision complexes. The insertion pathway into the carbon–hydrogen bond leads to i3 (C_s, $^2A'$). Note that all attempts to locate a one-step pathway to an insertion of silylidyne into the carbon–carbons single bond, i.e., intermediate i4 (C_s, $^2A'$), failed; i4 can be produced only via SiH addition to a triple bond in diacetylene forming i2 followed by the SiH migration toward the single C–C bond in i7 (C_s, $^2A'$) and the C–C bond rupture. Among the initial collision complexes, intermediate i3 connects to cis-i1 through a hydrogen migration via a transition state located $35\,kJ\,mol^{-1}$ above cis-i1. Our electronic structure calculations also reveal the existence of intermediates i5 (C_s, $^2A'$), i6 (C_1, ^2A), i8 (C_1, ^2A), and i9 (C_s, $^2A'$). Intermediate i5 essentially connects i3 with i2, whereas i6 can be accessed from

cis-i1, i3, and i2 via 1,2-hydrogen migration, 1,3-hydrogen migration, and 1,2-hydrogen migration accompanied with ring opening, respectively. These pathways are not competitive due to their high barriers and, in the case of i2 and i3, the transition states lie above our collision energy of $31.2 \pm 0.2\,kJ\,mol^{-1}$, such that the barriers cannot be overcome under our experimental conditions. This fate is shared with the transition states i2-i8, i8-i9, i6-i4, and i4-i9. Among all found intermediates, only i2 can undergo a unimolecular decomposition via atomic hydrogen loss yielding the 1-ethynyl-3-sila-cyclopropenylidene molecule (p1, C_s, X^1A') in a weakly exoergic reaction ($\Delta_r G = -17\,kJ\,mol^{-1}$). Intermediate i4 can emit atomic hydrogen from the silicon atom forming diethynylsilene (p2, C_{2v}, X^1A') in an overall endoergic reaction ($\Delta_r G = +21\,kJ\,mol^{-1}$). Note that both hydrogen atom eliminations were found to be barrierless, i.e., the reverse reactions of hydrogen atom addition to the silicon atom leading to i2 and i4 have no entrance barrier. While the hydrogen atom loss transition states i2-p1 and i4-p2 could be located at the ωB97XD/6-311G(d,p) level, their refined CCSD(T)-F12/cc-pVQZ-f12 energies, respectively, lie below those for the p1 and p2 products. For completion, we also explored the energetics of the hydrogen abstraction pathway $SiH + C_4H_2 \rightarrow SiH_2 + C_4H$. However, this direct channel is endoergic by $245\,kJ\,mol^{-1}$ and hence closed under our experimental conditions considering a collision energy of only $31.2 \pm 0.2\,kJ\,mol^{-1}$.

We are now merging our experimental findings with the results from the ab initio calculations to propose the underlying reaction mechanism(s) along with the chemical dynamics of the reaction. The reaction of the silylidyne radical with diacetylene
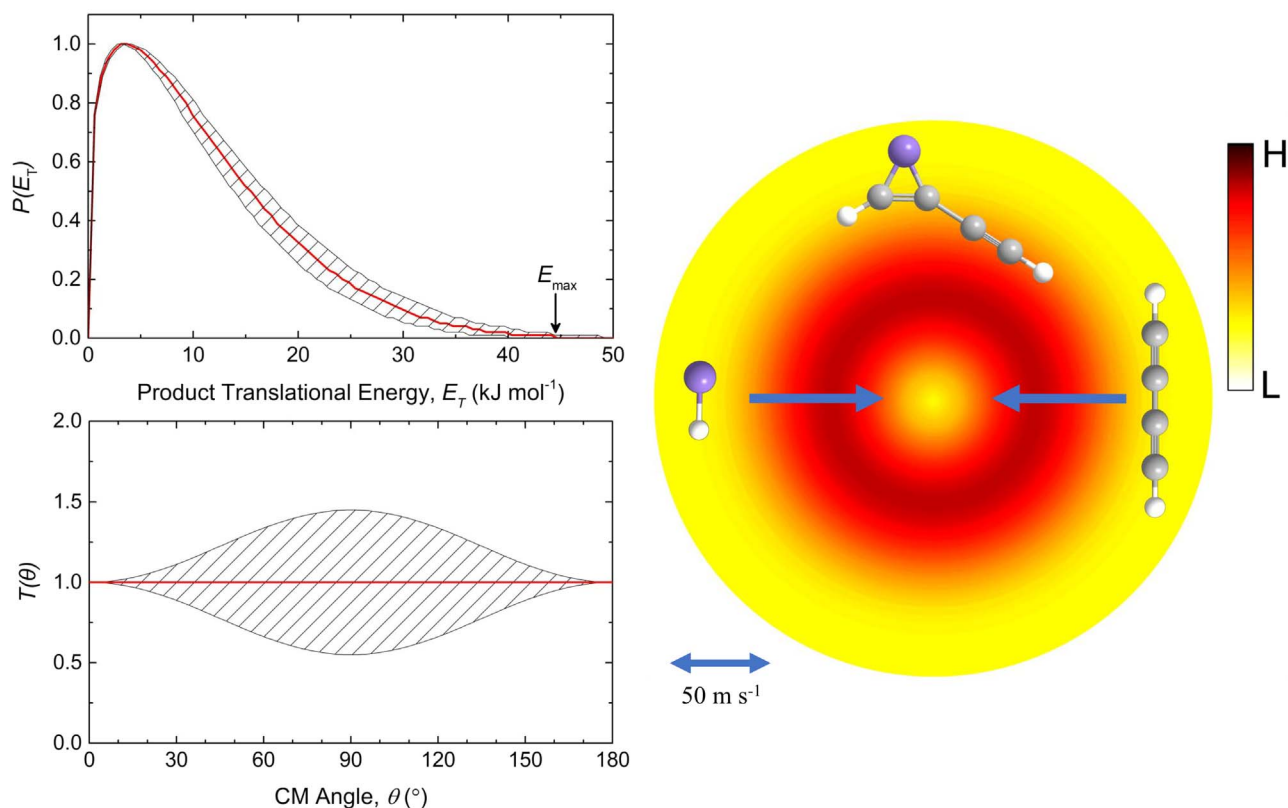
Figure 4. Translational energy flux distributions (top-left panel) and center-of-mass angular (bottom-left panel) and the top view of the flux contour map (right) leading to the synthesis of the 1-ethynyl-3-silacyclopropenylidene molecule (c-SiC$_4$H$_2$) plus atomic hydrogen in the reaction of the silylidyne radical with diacetylene. Hatched areas indicate the acceptable upper and lower error limits of the fits. The solid red lines define the best-fit function to replicate the laboratory data as shown in Figure 3. The flux contour map represents the flux intensity of the reactive scattering products as a function of the CM scattering angle (θ) and product velocity (u). The color bar indicates the flux gradient from high (H) intensity to low (L) intensity.

proceeds via indirect scattering dynamics (complex forming reaction) and is initiated by the barrierless addition of silylidyne radical to the π electron density leading either to the collision complex(es) i1 and/or i2. Collision complex i1 (cis/trans) undergoes facile ring closure to i2 with the latter ejecting a hydrogen atom to form 1-ethynyl-3-silacyclopropenylidene molecule (p1, C$_s$, X^{1}A$'$) in a weakly exoergic reaction ($\Delta_r G = -17$ kJ mol^{-1}). Product p2 is—if formed at all—only a minor contributor to the reactive scattering signal. The indirect reaction mechanism via a long-lived intermediate is also supported by the extracted CM angular distribution (Figure 4), which displays a forward–backward symmetry. Further, the loose exit transition state upon decomposition of i2 to 1-ethynyl-3-silacyclopropenylidene plus atomic hydrogen was predicted based on the CM translational energy distribution peaking close to zero translational energy. This simple bond-rupture process is connected with a weak electron "reorganization" considering the similar geometries and bond distances/angles of i2 and p1. Finally, the experimental reaction energy of -14 ± 5 kJ mol^{-1} correlates very well with the computationally derived exoergicity of 17 ± 3 kJ mol^{-1}.

3. Astrophysical Implications

Our combined experimental and computational study provided compelling evidence on the facile, barrierless formation of 1-ethynyl-3-silacyclopropenylidene molecule (c-SiC$_4$H$_2$) under single-collision conditions via the elementary gas phase reaction of the silylidyne radical with diacetylene. Because the reaction is exoergic and all isomerization barriers are located below the energy of the separated reactants, this mechanism is not only open in high-temperature circumstellar environments of carbon-rich AGB stars, where both the silylidyne and diacetylene reactants are readily available, but also in cold molecular clouds holding ultralow temperatures of 10 K such as toward TMC-1 and OMC-1. Therefore, both the C$_2$ and the C$_4$ hydrocarbons acetylene and diacetylene can be efficiently linked to the formation of hydrogen-deficient organosilicon species—silacyclopropenylidene and 1-ethynyl-3-silacyclopropenylidene—as the dominant carbon reservoir in carbon-rich outflows. This universal route may represent a versatile reaction mechanism to "access" hydrogen-poor organosilicon molecules through elementary neutral–neutral reactions involving the silylidyne radical with alkynes–hydrocarbons carrying a carbon–carbon triple bond. Note that although the bare silicon carbides have been observed in circumstellar envelopes (Figure 1), the existence of hydrogen-deficient silicon carbides is still elusive in deep space. Once synthesized, these organosilicon molecules might be photolyzed easily considering the relatively weaker carbon–hydrogen bond of about 400 kJmol^{-1} compared to bond strengths of carbon–carbon and carbon–silicon double bonds of 450–500 kJmol^{-1}. In case of silacyclopropenylidene (c-SiC$_2$H$_2$), matrix isolation studies revealed that silacyclopropenylidene can be easily photolyzed to the cyclic silicon dicarbide molecule (c-SiC$_2$) (Maier et al. 1994; Parker et al. 2013). Therefore, although not yet verified experimentally, these results predict that 1-ethynyl-3-silacyclo-propenylidene (c-SiC$_4$H$_2$) may degrade photochemically to the astronomically observed silicon tetracarbide (SiC$_4$; Ohishi et al. 1989; Job et al. 2020).
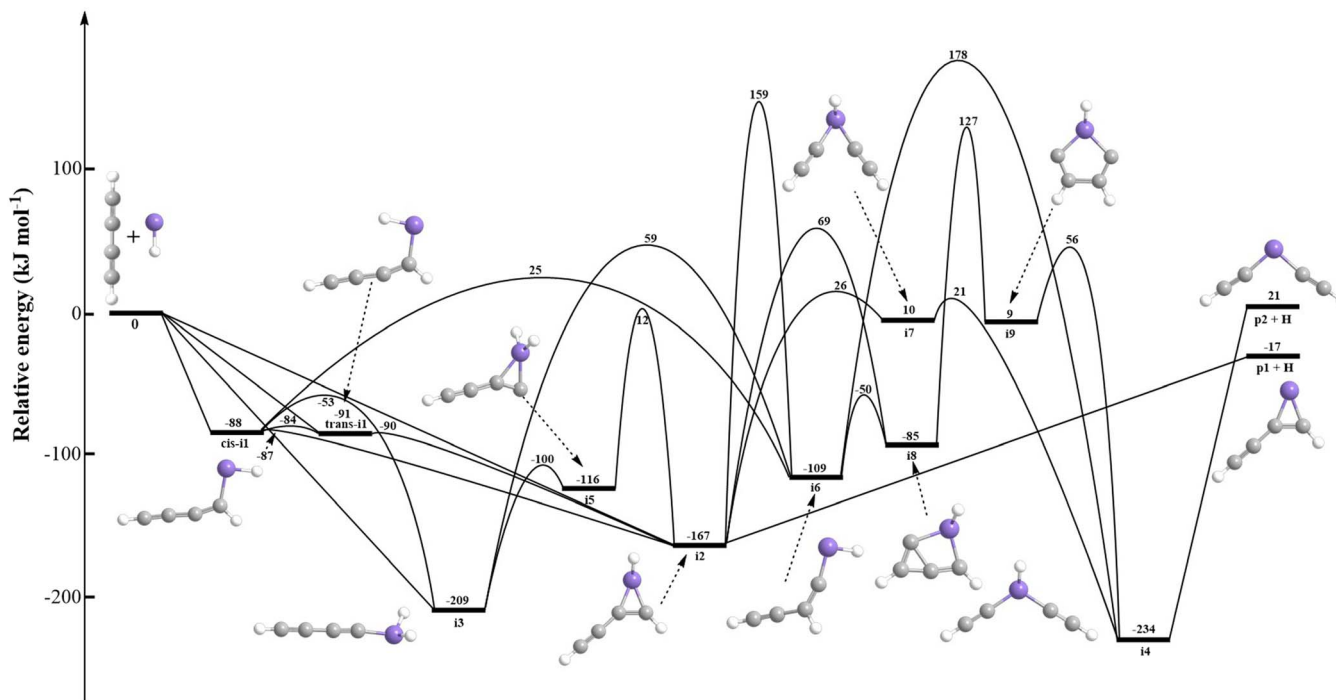
Figure 5. Potential energy surface of the reaction of the silylidyne radical (SiH) with diacetylene (C_4H_2) in the crossed molecular beam experiments leading to the 1-ethynyl-3-silacyclopropenylidene molecule (c-SiC_4H_2) plus atomic hydrogen. Relative energies calculated at the CCSD(T)-F12/cc-pVQZ-f12//ωB97XD/6-311G (d,p) + ZPE(ωB97XD/6-311G(d,p)) level are given in units of kJ mol^{-1}. The optimized cartesian coordinates for all structures are given in the Appendix (Table 1).

After nucleation and chemical growth in the circumstellar envelopes, silicon-carbide dust grains are processed in the ISM through energetic ions in shock waves (Jones et al. 1994). Since the sputtering by energetic ions is very efficient, the calculated lifetime of silicon-carbide dust grains in the ISM of about 5×10^8 yr is much shorter than the injection timescale of dust by stars of 2×10^9 yr. This consideration implies that only a small fraction of the silicon-carbide grains might be formed in circumstellar envelopes with hitherto undiscovered sources of a rapid chemical growth of dust in low temperature interstellar environments (Draine 2009). Overall, the inefficient formation of simple silicon-carbide grains and the ubiquitous presence grains in the ISM reveals crucial, but hitherto unexplained, reaction pathways leading to a supply of organosilicon species via a fast chemical growth. In other words, while grain growth in the ISM is often invoked to reconcile the large discrepancy of injection and destruction timescales with the observed high abundance of interstellar dust, chemical routes have never been identified. Fast reactions of silylidyne radicals with alkynes as presented here via the silylidyne–diacetylene system could represent this missing reaction class, thus providing the molecular feedstock of organosilicon molecules necessary to account for the ubiquitous presence of interstellar silicon-carbide grains via a "bottom up" synthesis starting with small silicon-bearing precursor molecules as proposed here. Prospective searches for 1-ethynyl-3-silacyclopropenylidene exploiting the Atacama Large Millimeter Array merged with laboratory astrophysics experiments as conducted here are expected to provide critical constraints and a comprehensive picture of the fundamental processes involved in the formation of organosilicon molecules at the molecular level and their link to silicon-carbide grain formation in the ISM.

Appendix

A.1. Experimental Methods

The crossed-beam experiments of ground-state silylidyne radicals (SiH, $X^2\Pi$) with diacetylene (C_4H_2, $X^1\Sigma_g^+$) were carried out under single-collision conditions in a crossed molecular beams machine (Gu et al. 2006). A pulsed supersonic beam of ground-state silylidyne radicals (SiH, $X^2\Pi$) was generated via photolysis of 0.5% disilane (Si_2H_6; 99.998%; Voltaix) seeded in helium (He; 99.9999%; Gaspro) at 193 nm. This pulsed beam of the silylidyne radicals passed through a skimmer and traversed a four-slit chopper wheel rotating at 120 Hz selecting a part of the supersonic beam with a well-defined peak velocity (v_p) and speed ratio (S) of 1738 ± 8 m s^{-1} and 17.0 ± 2.5, respectively (Table 2). The chopper wheel motor (2057S024B, Faulhaber) was interfaced to a precision motion controller (MC 5005 S RS, Faulhaber). Cables between the motor and the controller had to be shielded to ensure an interference-free operation of the motor. At frequencies of 480 Hz, the 2083.3 μs signal period was stable within ± 0.1 μs as determined via a digital oscilloscope (TDS 2024B, Tektronix). In the interaction region, this section of the pulse intersected the most intense part of a pulsed beam of diacetylene (99.5%+) seeded in argon (99.9999%; Gaspro) at a level of 5%. The peak velocity and speed ratio of the diacetylene pulse were determined to be 620 ± 20 m s^{-1} and 12.0 ± 0.3 yielding a nominal collision energy of 31.2 ± 0.2 kJ mol^{-1} as well as a CM angle of $31.5° \pm 0.1°$. To allow a "laser-on" minus "laser-off" background subtraction, both pulsed valves were triggered at 120 Hz, but the laser was

operated at half of the repetition rate at 60 Hz. The reactively scattered products were mass filtered after electron impact ionization utilizing a quadrupole mass spectrometer operated in the TOF mode; ions are monitored by a Daly-type detector housed in a rotatable, triply differentially pumped ultrahigh vacuum chamber (7×10^{-12} Torr). This complete detector assembly is rotatable within the plane spanned by both supersonic beams to record angular-resolved TOF spectra. To collect information on the scattering dynamics, the laboratory data were transformed from the laboratory into the CM reference frame exploiting a forward-convolution routine (Kaiser et al. 2002) yielding an angular flux distribution, $T(\theta)$, and translational energy flux distribution, $P(E_T)$, in the CM system. The laboratory TOF spectra and the angular distributions are then reconstructed from the $P(E_T)$ and $T(\theta)$ functions (Levine 2009).

A.2. Theoretical Methods

Molecular geometries of SiH, C_4H_2, various intermediates and transition states on the SiC_4H_3 potential energy surface, as well as possible SiC_4H_2 products, were optimized using the hybrid ωB97XD density functional theory method (Chai & Head-Gordon 2008) with the 6-311G(d,p) basis set. All transition states were verified by intrinsic reaction coordinate (IRC) calculations. Vibrational frequencies for all stationary structures were computed at the same ωB97XD/6-311G(d,p) level of theory. Optimized Cartesian coordinates and vibrational frequencies are compiled in Table 1. Single-point energies at the optimized geometries were recalculated employing the explicitly correlated coupled clusters method with single and double excitations and perturbative treatment of triple excitations, CCSD(T)-F12 (Adler et al. 2007;

Table 1
Optimized Cartesian Coordinates (Å), and Vibrational Frequencies (cm^{-1}) of Reactants, H Dissociation Products, Intermediates, Transition States Involved in the Silylidyne Radical (SiH) Plus Diacetylene (C_4H_2) Reaction

Species	Vibrational Frequencies (cm^{-1})	Cartesian Coordinates (Å)			
		Atom	X	Y	Z
Diacetylene	228.55, 529.34, 533.42	C	−1.888346	−0.000349	−0.000055
	667.76, 693.13, 693.96	C	−0.686602	0.000798	0.000030
	694.04, 912.50, 2144.28	C	1.888335	−0.000888	0.000163
		C	0.686612	0.001187	−0.000032
		H	−2.952150	−0.003007	0.000061
		H	2.952155	−0.001482	−0.000690
Silylidyne	2072.67	Si	0.000000	0.000000	0.101986
		H	0.000000	0.000000	−1.427802
i1-cis	65.62, 147.14, 236.25	C	2.889665	−0.442187	0.000312
	292.08, 375.55, 415.89	C	1.760725	0.034194	−0.000430
	545.60, 658.57, 658.99	C	−0.711616	0.889610	−0.000365
	705.54, 838.51, 932.59	C	0.577427	0.633119	0.001212
	1158.02, 1765.62, 2022.25	Si	−1.910092	−0.573424	−0.000110
	2109.79, 3103.52, 3470.67	H	3.852954	−0.893564	−0.001894
		H	−1.046493	1.928697	−0.002480
		H	−3.162385	0.304390	0.001537
i1-trans	54.84, 94.68, 223.41	C	2.842730	−0.444391	−0.015637
	321.01, 370.26, 414.65	C	1.719707	0.042928	−0.004223
	537.04, 659.83, 703.88	C	−0.740754	0.937030	0.053875
	714.24, 840.95, 919.96	C	0.538297	0.648725	−0.001177
	1184.27, 1770.81, 2029.71	Si	−1.993554	−0.473078	−0.032145
	2084.39, 3116.46, 3472.58	H	3.804902	−0.897683	−0.020296
		H	−1.071510	1.972386	−0.040914
		H	−0.983516	−1.557370	0.314211
i2	170.20, 190.96, 452.17	C	−2.707268	0.250964	0.018218
	465.10, 530.12, 599.54	C	−1.519193	0.063004	−0.000914
	669.18, 704.74, 709.18	C	0.743096	−1.132908	0.039571
	795.86, 862.63, 1006.72	C	−0.128088	−0.110383	−0.027394
	1104.23, 1611.19, 2070.48	H	−3.758609	0.409722	0.037425
	2223.84, 3222.74, 3480.84	H	0.629060	−2.204974	0.139258
		Si	1.610790	0.451229	−0.105246
		H	2.247208	1.053989	1.119877
i3	108.90, 112.13, 283.06	C	−3.288705	−0.000158	−0.010239
	297.81, 498.15, 537.19	C	−2.084980	0.000023	0.004236
	560.40, 610.13, 683.80	C	0.498880	0.000219	0.052259
	687.95, 698.32, 929.26	C	−0.718091	0.000284	0.021658
	1056.45, 2148.82, 2203.24	Si	2.295250	−0.000103	−0.094717
	2226.24, 2291.63, 3480.61	H	−4.352342	−0.000394	−0.024659
		H	2.888286	1.233874	0.471570
		H	2.887940	−1.234248	0.471640

Table 1
(Continued)

Species	Vibrational Frequencies (cm^{-1})	Cartesian Coordinates (Å)			
		Atom	X	Y	Z
i4	95.39, 225.47, 230.47	C	−2.545568	−0.769466	0.022137
	256.24, 383.60, 544.21	C	−1.505649	−0.154182	0.032554
	630.23, 695.04, 706.21	C	2.545638	−0.769378	0.022095
	706.72, 748.42, 749.51	C	1.505504	−0.154430	0.032225
	801.23, 2133.91, 2138.79	Si	0.000018	0.838350	−0.109810
	2223.55, 3466.42, 3466.99	H	−3.457588	−1.319348	0.030963
		H	3.457852	−1.318961	0.029612
		H	−0.000063	1.986143	0.822695
i5	155.05, 196.38, 425.42	C	2.700742	−0.318325	−0.000012
	430.37, 521.53, 563.98	C	1.547959	0.021630	−0.000046
	596.59, 654.96, 683.63	C	−0.751950	1.262411	−0.000001
	696.65, 768.19, 909.17	C	0.193319	0.362750	−0.000017
	996.25, 1751.34, 2241.01	Si	−1.547095	−0.386561	0.000021
	2248.72, 2259.95, 3485.58	H	3.725117	−0.604324	0.000093
		H	−2.103076	−0.977310	1.232639
		H	−2.103126	−0.977316	−1.232570
i6	91.36, 238.47, 283.08	C	−2.752550	−0.662768	0.042023
	292.64, 497.23, 516.68	C	−1.788500	0.052747	0.009139
	579.00, 696.85, 706.46	C	0.595121	0.509654	−0.010207
	733.50, 835.35, 1001.52	C	−0.659735	0.919776	−0.041324
	1251.56, 1694.98, 2079.39	Si	2.092651	−0.419124	−0.074481
	2234.52, 3117.22, 3483.30	H	−3.600363	−1.304162	0.071489
		H	−0.862823	1.990361	−0.103380
		H	2.800052	0.265077	1.076844
i7	205.34, 230.08, 266.83	C	−0.220893	0.910499	0.012090
	267.46, 296.78, 433.14	C	−1.245313	1.603460	0.001647
	575.86, 578.49, 588.67	C	−0.220946	−0.910191	0.012134
	657.90, 662.01, 699.94	C	−1.244950	−1.603802	0.001626
	771.18, 1783.71, 1932.48	Si	1.444362	0.000018	−0.110562
	2095.22, 3442.61, 3449.05	H	−2.120631	2.211336	−0.008493
		H	−2.120206	−2.211792	−0.008253
		H	1.612382	0.000415	1.399628
i8	262.40, 375.23, 454.86	C	1.783310	−0.134604	0.025844
	484.92, 605.18, 651.91	C	0.710495	−0.919665	−0.055445
	689.43, 734.38, 753.29	C	−0.552699	1.262418	0.015068
	770.64, 974.90, 1086.14	C	0.657627	0.673128	0.057393
	1098.68, 1488.33, 1745.50	Si	−1.137141	−0.454391	−0.099152
	2141.59, 3262.76, 3267.39	H	2.861501	−0.138040	0.039116
		H	−0.801370	2.310932	−0.016518
		H	−1.732551	−1.099074	1.108376
i9	17.20, 276.18, 446.69	C	1.254862	−0.757652	−0.009389
	521.16, 562.19, 655.30	C	0.048201	−1.315450	0.064076
	668.42, 769.25, 829.97	C	1.252311	0.761283	0.006172
	849.74, 915.04, 1181.98	C	0.042670	1.315414	0.040880
	1203.40, 1537.38, 1595.60	Si	−1.252069	−0.002691	−0.099529
	2236.86, 3167.76, 3181.50	H	2.205657	−1.284321	−0.019681
		H	2.200625	1.290102	0.058526
		H	−2.465585	0.010319	0.744127
i1-cis-i1-trans	278.59i, 84.80, 222.57	C	−2.739842	−0.459046	0.000911
	253.46, 399.44, 480.10	C	−1.627198	0.052186	0.005268
	513.01, 558.47, 604.79	C	0.778574	1.075438	−0.008605
	626.56, 771.44, 900.41	C	−0.435152	0.644781	0.015997
	986.30, 1806.15, 1993.67	H	−3.696925	−0.920245	−0.006811
	2036.90, 3110.80, 3467.29	H	1.129903	2.104345	0.028974
		Si	1.767647	−0.597915	−0.108103
		H	1.961671	−0.693441	1.409862
i1-cis-i3	1405.75i, 110.57, 113.37	C	3.252678	−0.039738	0.019736
	292.99, 366.48, 479.37	C	2.041976	0.012399	−0.011917

Table 1
(Continued)

Species	Vibrational Frequencies (cm^{-1})	Cartesian Coordinates (Å)			
		Atom	X	Y	Z
	522.30, 532.87, 636.66	C	−0.553912	0.125712	−0.059648
	670.42, 747.10, 821.89	C	0.697980	0.071926	−0.052402
	1053.93, 1728.23, 1953.29	Si	−2.358479	−0.107768	−0.068047
	2082.91, 2119.10, 3473.77	H	4.315109	−0.087895	0.049274
		H	−1.286822	−0.679036	1.004719
		H	−2.641923	1.253885	0.524053
i3-i5	385.46i, 146.62, 198.15	C	2.745406	−0.397766	0.000008
	280.95, 436.06, 497.30	C	1.628806	0.046161	−0.000024
	610.93, 666.03, 669.84	C	−0.730815	1.190703	0.000027
	732.41, 746.98, 879.97	C	0.340750	0.539408	−0.000026
	915.90, 1954.27, 2203.90	Si	−1.628984	−0.447364	0.000004
	2235.64, 2265.25, 3478.61	H	3.736188	−0.786118	0.000090
		H	−2.417692	−0.610919	1.242396
		H	−2.417603	−0.610900	−1.242456
i5-i2	767.94i, 163.81, 202.45	C	−2.623618	−0.317597	−0.006812
	437.96, 461.09, 486.20	C	−1.462680	−0.012003	0.008552
	525.58, 642.20, 677.34	C	0.586787	1.450166	−0.097728
	684.67, 699.47, 816.81	C	−0.096741	0.316123	0.038598
	1039.84, 1637.93, 2077.45	Si	1.519544	−0.540691	0.103797
	2100.84, 2251.67, 3486.57	H	−3.655485	−0.573674	−0.027558
		H	1.834965	−1.351775	−1.114057
		H	2.124414	0.875000	0.032801
i1-cis-i2	−201.20, 77.60, 203.25	C	2.772044	−0.411165	0.035151
	316.56, 349.24, 463.06	C	1.643902	0.056233	0.012761
	509.31, 615.47, 681.59	C	−0.800517	1.033115	−0.085831
	702.52, 796.70, 886.90	C	0.412327	0.563965	−0.009237
	1061.55, 1778.90, 2038.77	Si	−1.730868	−0.607415	−0.072563
	2079.19, 3132.26, 3471.21	H	3.750867	−0.827130	0.049699
		H	−1.087120	2.060736	0.132809
		H	−2.598120	−0.182683	1.116308
i1-trans-i2	166.15i, 96.52, 202.38	C	2.731180	−0.375304	−0.039703
	372.74, 398.59, 488.11	C	1.600958	0.068257	−0.008458
	527.18, 630.57, 699.97	C	−0.819330	1.087871	0.092139
	718.74, 767.72, 872.26	C	0.326762	0.501699	0.037691
	1020.49, 1804.46, 2084.61	Si	−1.756634	−0.552575	−0.094351
	2099.44, 3176.41, 3473.64	H	3.726169	−0.749927	−0.069254
		H	−1.108028	2.113573	−0.114075
		H	−1.062688	−1.322728	1.014229
i2-i7	359.87i, 212.03, 252.87	C	1.505953	1.417244	0.002774
	267.28, 295.40, 425.46	C	0.541126	0.674329	−0.021135
	500.27, 595.19, 632.56	H	2.325464	2.096670	0.017479
	663.91, 668.07, 729.83	C	0.869288	−1.823290	0.000179
	773.88, 1719.88, 1988.21	C	0.031916	−0.890425	0.033810
	2094.87, 3426.50, 3454.69	H	1.718434	−2.466325	−0.021468
		Si	−1.444276	0.264994	−0.106453
		H	−1.513725	0.392589	1.400568
i7-i4	490.10i, 201.96, 237.27	C	1.337626	−1.577300	0.005260
	274.68, 284.13, 430.46	C	0.267550	−0.959198	0.010059
	523.71, 551.37, 565.03	C	1.145517	1.712768	−0.004994
	587.06, 640.12, 667.51	C	0.140193	0.987303	0.040294
	746.46, 1742.09, 1907.27	Si	−1.422400	−0.078781	−0.117188
	2040.58, 3436.60, 3442.05	H	2.233558	−2.152491	−0.004279
		H	1.992340	2.357458	−0.043518
		H	−1.657615	−0.083466	1.384707
i2-p1	226.64i, 40.32, 68.34	C	2.705231	−0.258207	0.010104
	167.89, 202.46, 461.38	C	1.518408	−0.060290	−0.004208
	480.85, 593.48, 632.49	C	−0.748563	1.118632	0.194245
	746.24, 777.49, 889.40	C	0.129297	0.122780	−0.034421

Table 1
(Continued)

Species	Vibrational Frequencies (cm^{-1})	Cartesian Coordinates (Å)			
		Atom	X	Y	Z
	988.29, 1091.11, 1596.62	Si	−1.610185	−0.404451	−0.282107
	2219.61, 3210.64, 3484.42	H	3.755181	−0.426048	0.024768
		H	−0.638843	2.154651	0.491863
		H	−2.199982	−1.603771	2.438544
i4-p2	211.90i, 49.19, 55.59	C	−2.403853	−0.849943	0.090707
	92.97, 170.41, 185.10	C	−1.383142	−0.210899	−0.035397
	246.56, 424.28, 622.66	C	2.403914	−0.849863	0.090802
	630.74, 674.36, 675.10	C	1.383195	−0.210830	−0.035285
	783.13, 783.27, 2121.04	Si	0.000010	0.982020	−0.283115
	2127.28, 3466.21, 3466.60	H	−3.289023	−1.431435	0.206583
		H	3.289071	−1.431382	0.206643
		H	−0.000863	1.843749	2.885423
i1-cis-i6	680.75i, 82.91, 125.33	C	3.239487	0.064780	−0.038791
	212.71, 297.17, 328.97	C	2.030191	0.024495	−0.003546
	398.43, 465.12, 522.05	C	−0.597571	−0.069054	0.021821
	622.12, 768.47, 812.42	C	0.679319	−0.019127	0.065080
	1007.99, 1881.15, 2079.16	Si	−2.409646	0.169312	−0.011249
	2146.92, 2414.64, 3473.74	H	4.301885	0.105760	−0.083133
		H	−0.042320	−1.160854	0.199870
		H	−2.633075	−1.321849	−0.226640
i6-i8	96.55i, 246.32, 368.91	C	−0.623618	−1.601226	−0.003149
	423.13, 535.66, 553.31	C	−1.123683	−0.489056	0.007445
	589.03, 647.00, 713.33	C	0.008095	1.344831	0.060161
	750.37, 774.46, 997.65	C	−1.256834	0.935439	−0.010164
	1206.69, 1585.15, 2071.31	Si	1.357800	0.013169	−0.119568
	2105.45, 3219.07, 3461.54	H	−0.351778	−2.630456	0.033751
		H	−2.196152	1.469692	−0.067975
		H	1.514979	−0.163538	1.382418
i2-i8	271.16i, 223.99, 265.67	C	1.925083	0.110545	−0.374039
	338.23, 496.46, 529.11	C	1.666770	−0.830498	0.426947
	647.79, 702.12, 758.29	C	−0.394296	1.079723	0.311513
	802.42, 885.13, 918.71	C	0.307052	−0.056065	0.116646
	1035.63, 1484.96, 1810.26	Si	−1.491107	−0.272198	−0.231832
	2120.87, 3198.82, 3374.53	H	2.263382	0.883003	−1.034549
		H	−0.123289	2.093020	0.585328
		H	−2.292239	−0.987477	0.808462
i8-i9	786.92i, 285.61, 365.14	C	−0.301770	1.499077	−0.125529
	374.32, 474.67, 530.44	C	0.818648	0.849915	0.003450
	594.38, 624.49, 733.35	C	0.507523	−1.222047	0.095271
	754.92, 816.56, 946.62	C	1.548955	−0.404060	−0.054502
	1181.53, 1540.06, 1730.65	Si	−1.211694	−0.352103	−0.119615
	2088.35, 2433.35, 3250.77	H	0.549754	1.472779	1.004802
		H	2.616481	−0.519623	−0.166157
		H	−1.642661	−0.361029	1.323817
i4-i9	997.08i, 165.15, 261.44	C	1.247798	−0.969239	−0.011638
	392.31, 453.55, 574.83	C	0.042540	−1.364054	0.065019
	634.47, 678.82, 706.74	C	1.216255	0.994725	0.028885
	718.20, 777.42, 785.44	C	−0.003936	1.368224	−0.001342
	953.13, 1596.76, 1738.64	Si	−1.227586	−0.018458	−0.101977
	2210.30, 3284.90, 3295.75	H	2.280814	−1.271347	−0.066117
		H	2.232824	1.339156	0.135616
		H	−2.343372	0.012665	0.872626
s i4-i6	117.03i, 22.34, 50.65	C	1.854359	0.095323	−0.083695
	62.06, 117.83, 182.43	C	2.776272	−0.661380	0.062465
	253.93, 592.16, 644.09	C	−0.892773	0.784002	0.017741
	649.57, 691.31, 802.97	C	−0.325948	1.858737	0.001590
	851.22, 2095.98, 2108.84	Si	−1.532189	−0.953550	−0.064758
	2113.85, 3467.97, 3484.28	H	3.606241	−1.318373	0.177498

Table 1
(Continued)

Species	Vibrational Frequencies (cm^{-1})	Cartesian Coordinates (Å)			
		Atom	X	Y	Z
		H	0.144517	2.815714	0.004119
		H	−2.771579	−0.607724	0.736394
i2-i6	491.14*i*, 169.46, 214.93	C	2.688562	−0.264957	−0.063872
	312.48, 450.65, 513.47	C	1.511342	−0.051411	0.034706
	583.72, 645.38, 689.43	C	−0.731469	1.306620	−0.102214
	712.89, 762.86, 957.68	C	0.107082	0.152058	0.134711
	1003.69, 1316.46, 2112.17	Si	−1.623163	−0.425797	−0.146434
	2235.14, 2415.25, 3482.19	H	3.732133	−0.445526	−0.162468
		H	−0.193566	0.650990	1.172037
		H	−2.267390	−1.098164	1.020518
i3-i6	433.47*i*, 147.08, 233.17	C	2.762774	−0.207903	−0.038477
	398.59, 466.42, 560.38	C	1.574417	−0.038637	0.011763
	651.75, 687.26, 730.67	C	−0.663221	1.189586	−0.104095
	742.54, 766.08, 924.36	C	0.175824	0.146741	0.095466
	1091.81, 1567.82, 1826.27	Si	−1.753912	−0.289335	0.078549
	2053.53, 2226.60, 3482.89	H	3.816020	−0.343658	−0.098989
		H	−0.238650	−1.036742	0.342742
		H	−2.121369	−1.107634	−1.131374
p1	167.81, 195.26, 465.31	C	−2.659442	−0.212757	−0.000043
	476.16, 596.07, 643.19	C	−1.466988	−0.051382	0.000111
	724.83, 790.89, 875.33	C	0.826903	1.090838	−0.000020
	991.60, 1096.12, 1599.80	C	−0.072368	0.087235	0.000032
	2219.63, 3214.84, 3480.50	Si	1.657795	−0.521882	−0.000016
		H	−3.714278	−0.347932	−0.000216
		H	0.736518	2.170672	−0.000046
p2	94.17, 172.61, 189.60	C	−2.402402	−0.821144	−0.000081
	247.47, 425.66, 620.45	C	−1.382448	−0.168509	−0.000186
	627.54, 676.40, 677.45	C	2.402402	−0.821143	−0.000082
	796.21, 796.33, 2117.59	C	1.382449	−0.168508	−0.000188
	2124.03, 3463.12, 3463.52	Si	0.000000	1.050692	0.000098
		H	−3.285625	−1.416927	0.000922
		H	3.285621	−1.416933	0.000933
p3	91.29, 109.36, 272.96	C	−3.217949	−0.013804	0.000040
	295.81, 479.35, 542.08	C	−2.014194	0.001228	−0.000168
	580.10, 656.04, 734.49	C	0.571839	0.055900	0.000532
	826.42, 1037.85, 2108.38	C	−0.648085	0.018647	−0.000220
	2139.57, 2296.95, 3480.26	Si	2.392784	−0.123051	−0.000078
		H	−4.281707	−0.028080	0.000189
		H	2.633064	1.378968	−0.000201
p4	192.49, 289.70, 530.53	C	2.402617	0.000002	−0.000838
	541.14, 621.25, 710.32	C	1.080772	−0.000007	0.000569
	872.86, 1021.29, 1089.96	C	−0.142750	−0.729714	0.001200
	1108.92, 1157.27, 1456.08	C	−0.142748	0.729714	0.001197
	1861.22, 3178.92, 3278.82	Si	−1.791893	0.000001	−0.000725
		H	2.949572	0.933619	−0.001305
		H	2.949591	−0.933603	−0.001318
p5	109.63, 179.52, 310.33	C	2.784283	−0.569468	0.000250
	330.87, 533.85, 692.02	C	1.758413	0.056575	0.000119
	728.46, 812.29, 865.60	C	−0.661612	0.316259	−0.000076
	1025.58, 1313.90, 1762.09	C	0.564353	0.831704	−0.000032
	2228.61, 3109.85, 3480.58	Si	−2.219129	−0.327725	−0.000130
		H	3.684444	−1.136237	0.000352
		H	0.710744	1.913973	−0.000104
p6	122.62, 155.54, 459.67	C	2.039499	0.661308	0.000297
	498.78, 572.17, 754.78	C	2.039435	−0.661473	0.000284
	904.93, 929.02, 958.41	C	−0.554054	0.000427	−0.001195
	1108.81, 1276.48, 1592.90	C	0.774395	−0.000014	−0.000501
	1833.78, 3254.41, 3294.62	Si	−2.214982	−0.000116	0.000388

Table 1
(Continued)

Species	Vibrational Frequencies (cm^{-1})	Cartesian Coordinates (Å)			
		Atom	X	Y	Z
		H	2.606829	1.578768	0.000614
		H	2.607275	−1.578630	0.000645
p7	126.35, 138.76, 227.29	C	2.505233	−0.343553	0.000364
	333.92, 368.68,638.71	C	1.346207	−0.009492	0.000580
	640.94, 736.77, 786.32	C	−1.739637	−0.530519	−0.626802
	840.46, 916.05, 1897.85	C	−1.741751	−0.527309	0.627572
	2172.27, 2263.49, 3465.38	Si	−0.381615	0.509277	−0.000620
		H	3.527023	−0.647555	0.000478
		H	−0.404731	1.982913	−0.002080
p8	110.86, 225.27, 255.48	C	−1.804594	−0.000007	0.630572
	400.10, 638.27, 728.03	C	−1.805548	0.000006	−0.630751
	752.67, 948.34, 1049.56	Si	−0.095972	0.000001	0.000178
	1054.23, 1204.24, 1471.64	C	1.529222	0.683848	0.000213
	1862.91, 3209.42, 3226.96	C	1.529221	−0.683850	0.000206
		H	2.326905	1.417801	−0.001960
		H	2.326902	−1.417803	−0.001976
p9	69.27, 87.31, 210.73	C	3.395858	0.000208	−0.000026
	210.78, 533.95, 565.91	C	2.126492	−0.000068	0.000448
	592.47, 624.98, 666.82	C	−0.436047	−0.000248	−0.000614
	973.43, 1209.69, 1961.86	C	0.821536	−0.000164	−0.000210
	2218.10, 2275.33, 2292.81	Si	−2.116304	0.000082	0.000115
		H	−2.909143	1.240328	0.000401
		H	−2.909640	−1.239843	0.000402
p10	86.70, 113.53, 131.33	C	−2.582754	−0.031971	−0.000043
	168.04, 415.52, 442.46	C	−1.284350	0.187054	−0.000028
	629.17, 983.50, 1028.18	C	1.975566	0.698374	0.000007
	1030.62, 1455.61, 1736.98	C	2.118208	−0.575304	0.000069
	1804.89, 3102.03, 3176.67	Si	0.353406	−0.102531	−0.000039
		H	−3.290308	0.797542	0.000383
		H	−3.017401	−1.031034	0.000128

Table 2
Peak Velocity (v_p) and Speed Ratios (S) of the Silylidyne (SiH) and Diacetylene (C_4H_2) Beams along with the Corresponding Collision Energy (E_C) and CM Angle Θ_{CM}

Beam	v_p (m s^{-1})	S	E_c (kJ mol^{-1})	Θ_{CM} (deg)
SiH	1738 ± 8	17.0 ± 2.5		
C_4H_2	620 ± 20	12.0 ± 0.3	31.2 ± 0.2	31.5 ± 0.1

Knizia et al. 2009), with Dunning's correlation-consistent cc-pVQZ-f12 basis set (Dunning 1989) providing a close approximation to CCSD(T) energies at the complete basis set limit. This theoretical method was demonstrated to be capable of predicting relative energies of the local minima and transition states within $8\,\text{kJ mol}^{-1}$ and reaction energies to a precision of $3\,\text{kJ mol}^{-1}$ (Zhang & Valeev 2012). The discussion in this Letter is based upon final energies evaluated at the CCSD(T)-F12/cc-pVQZ-f12//ωB97XD/6-311G(d,p) level including zero-point vibrational energy corrections (ZPE) computed at ωB97XD/6-311G(d,p). The electronic structure calculations were carried out using the GAUSSIAN 09 (Frisch et al. 2009) and MOLPRO 2015 (Werner et al. 2010) quantum chemistry program packages.

ORCID iDs

Ralf I. Kaiser https://orcid.org/0000-0002-7233-7206

References

Adler, T. B., Knizia, G., & Werner, H.-J. 2007, JChPh, 127, 221106
Apponi, A., McCarthy, M., Gottlieb, C., & Thaddeus, P. 1999, ApJ, 516, L103
Bernath, P., Rogers, S., O'Brien, L., Brazier, C., & McLean, A. 1988, PhRvL, 60, 197
Chai, J.-D., & Head-Gordon, M. 2008, PCCP, 10, 6615
Cherchneff, I. 2012, A&A, 545, A12
Cherchneff, I., Le Teuff, Y., Williams, P., & Tielens, A. 2000, A&A, 357, 572
Decin, L., Cherchneff, I., Hony, S., et al. 2008, A&A, 480, 431
Draine, B. T. 2009, in ASP Conf. Ser. 414, Cosmic Dust—Near and Far, ed. T. Henning, E. Grün, & J. Steinacker (San Francisco, CA: ASP), 453
Dunning, T. H., Jr. 1989, JChPh, 90, 1007
Frisch, M., Trucks, G., Schlegel, H., et al. 2009, Gaussian 09 Revision D. 01 (Wallingford CT: Gaussian, Inc.)
Goldhaber, D., & Betz, A. 1984, ApJL, 279, L55
Gu, X., Guo, Y., Zhang, F., Mebel, A. M., & Kaiser, R. I. 2006, FaDi, 133, 245
Job, N., Karton, A., Thirumoorthy, K., Cooksy, A. L., & Thimmakondu, V. S. 2020, JPCA, 124, 987
Jones, A., Tielens, A., Hollenbach, D., & McKee, C. 1994, ApJ, 433, 797
Kaiser, R. I., Le, T. N., Nguyen, T. L., et al. 2002, FaDi, 119, 51
Knizia, G., Adler, T. B., & Werner, H.-J. 2009, JChPh, 130, 054104
Levine, R. D. 2009, Molecular Reaction Dynamics (Cambridge: Cambridge Univ. Press)

Li, X., Millar, T. J., Walsh, C., Heays, A. N., & Van Dishoeck, E. F. 2014, A&A, 568, A111

Lis, D. C., Blake, G. A., & van der Hucht, K. A. 2006, Astrochemistry: Recent Successes and Current Challenges (IAU S231) (Cambridge: Cambridge Univ. Press)

Maier, G., Reisenauer, H. P., & Meudt, A. 1998, Eur. J. Org. Chem., 1998, 1285

Maier, G., Reisenauer, H. P., & Pacl, H. 1994, Angew. Chem. Int. Ed. Engl., 33, 1248

Massalkhi, S., Agúndez, M., Cernicharo, J., et al. 2018, A&A, 611, A29

McCarthy, M., Gottlieb, C., & Thaddeus, P. 2003, MolPh, 101, 697

McCarthy, M., & Thaddeus, P. 2002, JMoSp, 211, 228

McCarthy, M. C., Gottlieb, C. A., & Cernicharo, J. 2019, JMoSp, 356, 7

McElroy, D., Walsh, C., Markwick, A., et al. 2013, A&A, 550, A36

Merrill, P. W. 1926, PASP, 38, 175

Millar, T. J., & Herbst, E. 1994, A&A, 288, 561

Ohishi, M., Kaifu, N., Kawaguchi, K., et al. 1989, ApJL, 345, L83

Parker, D. S., Wilson, A. V., Kaiser, R. I., et al. 2013, ApJ, 770, 33

Redman, M., Viti, S., Cau, P., & Williams, D. 2003, MNRAS, 345, 1291

Sanford, R. 1926, PASP, 38, 177

Speck, A., Barlow, M., & Skinner, C. 1997, M&PS, 32, 703

Suto, M., & Lee, L. 1986, JChPh, 84, 1160

Thaddeus, P., Cummins, S., & Linke, R. 1984, ApJL, 283, L45

Velilla-Prieto, L., Cernicharo, J., Agúndez, M., et al. 2018, PIAU, 14, 535

Wakelam, V., Smith, I., Herbst, E., et al. 2010, SSRv, 156, 13

Weltner, W., Jr., & McLeod, D., Jr. 1964, JChPh, 41, 235

Werner, H.-J., Knowles, P., Lindh, R., et al. 2010, MOLPRO, Version 2010.1, A Package of Ab Initio Programs (Cardiff: Univ. Cardiff), http://www.molpro.net

Willacy, K., & Cherchneff, I. 1998, A&A, 330, 676

Yang, T., Bertels, L., Dangi, B. B., et al. 2019, PNAS, 116, 14471

Yang, T., Dangi, B. B., Maksyutenko, P., et al. 2015, JPCA, 119, 12562

Yasuda, Y., & Kozasa, T. 2012, ApJ, 745, 159

Zhang, J., & Valeev, E. F. 2012, J. Chem. Theory Comput., 8, 3175

Zinner, E. 1995, in AIP Conf. Proc. 327, Nuclei in the Cosmos III, ed. M. Busso, C. M. Raiteri, & R. Gallino (Melville, NY: AIP), 567

Zinner, E. 1998, AREPS, 26, 147

Zinner, E., Nittler, L. R., Gallino, R., et al. 2006, ApJ, 650, 350

Ziurys, L. M. 2006, PNAS, 103, 12274